

This work was written as part of one of the author's official duties as an Employee of the United States Government and is therefore a work of the United States Government. In accordance with 17 U.S.C. 105, no copyright protection is available for such works under U.S. Law.

Public Domain Mark 1.0

<https://creativecommons.org/publicdomain/mark/1.0/>

Access to this work was provided by the University of Maryland, Baltimore County (UMBC) ScholarWorks@UMBC digital repository on the Maryland Shared Open Access (MD-SOAR) platform.

**Please provide feedback**

Please support the ScholarWorks@UMBC repository by emailing [scholarworks-group@umbc.edu](mailto:scholarworks-group@umbc.edu) and telling us what having access to this work means to you and why it's important to you. Thank you.

# Enhanced Performance of Dispenser Printed MA n-type $\text{Bi}_2\text{Te}_3$ Composite Thermoelectric Generators

Deepa Madan,<sup>\*,†</sup> Zuoqian Wang,<sup>†</sup> Alic Chen,<sup>†</sup> Rei-cheng Juang,<sup>‡</sup> Jay Keist,<sup>§,⊥</sup> Paul K. Wright,<sup>†</sup> and Jim W. Evans<sup>§</sup>

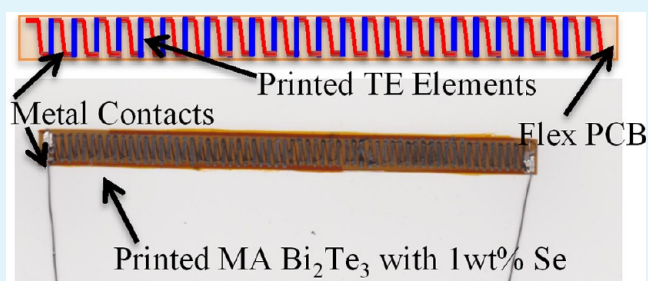
<sup>†</sup>Department of Mechanical Engineering and <sup>§</sup>Department of Materials Science and Engineering, University of California, Berkeley, California 94720, United States

<sup>‡</sup>Green Energy & Environment Research Laboratory, Industrial Technology Research Institute, Taiwan 310, R.O.C

<sup>⊥</sup>Physical and Life Sciences Directorate, Lawrence Livermore National Laboratory, Livermore, California 94550, United States

**ABSTRACT:** This work presents performance advancements of dispenser printed composite thermoelectric materials and devices. Dispenser printed thick films allow for low-cost and scalable manufacturing of microscale energy harvesting devices. A maximum  $ZT$  value of 0.31 has been achieved for mechanically alloyed (MA) n-type  $\text{Bi}_2\text{Te}_3$ -epoxy composite films with 1 wt % Se cured at 350 °C. The enhancement of  $ZT$  is a result of increase in the electrical conductivity through the addition of Se, which ultimately lowers the sintering temperature (350 °C). A 62 single-leg thermoelectric generator (TEG) prototype with 5 mm  $\times$  700  $\mu\text{m}$   $\times$  120  $\mu\text{m}$  printed element dimensions was fabricated on a custom designed polyimide substrate with thick metal contacts. The prototype device produced a power output of 25  $\mu\text{W}$  at 0.23 mA current and 109 mV voltage for a temperature difference of 20 °C, which is sufficient for low power generation for autonomous microsystem applications.

**KEYWORDS:** dispenser-printer, mechanically alloyed  $\text{Bi}_2\text{Te}_3$ , composite thermoelectric materials, energy harvesting, thermoelectric generators, Se additive



## INTRODUCTION

The global demand for affordable and renewable energy resources has led to important research approaches including thermoelectric (TE) energy conversion. Thermoelectric power generation provides solid-state conversion of heat into electrical power by utilizing the Seebeck effect.<sup>1</sup> The bulk of the thermoelectric research has been focused on inorganic TE semiconductor materials, conducting oxides, and metal alloys;<sup>2,3</sup> less attention has been paid to organic or polymer thermoelectric composite materials or slurries. Though the figure of merit ( $ZT$ ) of these composite materials is typically lower than that of inorganic materials, these materials enable the use of more scalable and cost-effective manufacturing methods.<sup>4–8</sup>

TEG device design is dependent on both the geometry and thermoelectric material properties.<sup>9,10</sup> The device electrical resistance must be low to maximize power output, thus requiring short element lengths. However, small element lengths pose difficulties in maintaining temperature differences across the device. Therefore, a trade-off occurs between device element length and power output, which ultimately depend on the TEG application. Furthermore, the voltage requirements of the application will dictate the array density of the device.

The customization required for enabling various TEG applications may be challenging for existing mass-production

pick and place techniques.<sup>11</sup> Applications involving waste-heat energy generation, in particular, require low-cost devices in order to be competitive. Traditional pick and place methods are labor, materials and energy intensive. This method has limited cost-effective scalability for manufacturing of application-specific TEGs. Alternatively, conventional microfabrication processes involving lithography and thin-film deposition are limited to the microscale regime.<sup>12,13</sup> The limitations of the available manufacturing technologies provide an opportunity for additive manufacturing methods such as direct-write printing.

Printing involves the deposition of synthesized thermoelectric inks, which consist of active TE materials in organic or polymer binders in slurry form. It eliminates the need for expensive processing steps such as lithography, physical and chemical vapor deposition and etching. It utilizes additive processing steps, thus reducing materials waste and cost per unit area. Printing is also an automated process that requires minimal labor in scaled manufacturing. Although the  $ZT$  of inorganic composite materials may be lower than that of conventional materials, the reduction of manufacturing costs associated with printing is significant.<sup>14</sup> As a result, the cost of

**Received:** August 23, 2012

**Accepted:** November 7, 2012

**Published:** November 7, 2012

energy generated from TEGs is improved through printed manufacturing.

In this work, we utilize a custom developed dispenser printer to print high aspect ratio planar single-element TEGs. The printer has been successfully used in battery, capacitor, TEGs, and microelectromechanical systems (MEMS) research.<sup>15–18</sup> We have reported in our previous work that p-type composite thermoelectric thick films have  $ZT$  of 0.41, whereas n-type thermoelectric composite thick films have  $ZT$  of 0.18, when cured at 350 °C. Electrical conductivity and overall  $ZT$  were higher for p-type  $\text{Sb}_2\text{Te}_3$ /epoxy composite films as compared to stock  $\text{Bi}_2\text{Te}_3$ /epoxy composite films.<sup>19</sup> This work focuses on optimizing the synthesis and processing parameters to maximize the  $ZT$  of n-type composite thermoelectric thick films for dispenser printing. Additionally, we demonstrate device fabrication techniques and enhanced device performance for high-density arrays of high aspect ratio planar single-element TEGs.

## EXPERIMENTAL SECTION

Elemental Bi (99.999%, 1–5 mm balls) and Te (99.999%, 1–12 mm chunks) (Sigma Aldrich Corporation) were selected as starting materials for mechanical alloying. A molar ratio of 36:64 of Bi and Te was used to form mechanically alloyed (MA) n-type  $\text{Bi}_2\text{Te}_3$ .<sup>1</sup> Varying amount of Se, 1–6 wt % of the total weight of  $\text{Bi}_2\text{Te}_3$ , was added. Se has been chosen as a dopant to improve the overall thermoelectric properties of the MA  $\text{Bi}_2\text{Te}_3$ .<sup>20–22</sup> Previous empirical studies have suggested that an average particle size of 10  $\mu\text{m}$  is needed to dispenser print inks.<sup>23–25</sup> Stainless steel jars containing 100 mL of isopropanol and 10 mm diameter balls were used for the ball-milling process. The ball to powder weight ratio was kept at 15:1. All powder handling was performed in an argon-filled glovebox, in which the oxygen level was kept below 5 ppm to prevent oxidation of the powders. Mechanical alloying was carried out in a planetary ball mill apparatus (Torrey Hills ND 0.4) at 315 rpm for 14 h in a purified argon atmosphere. The particle size of the as-milled powders was measured using a Coulter LS-100 laser diffraction particle size analyzer. The milled particle size ranged between 1 and 200  $\mu\text{m}$ . To further reduce the particle size, the as-milled powders were ball milled again with 3 mm stainless steel balls at a ball-to-powder mass ratio of 10:1 with isopropyl alcohol (1:1 fluid to powder ratio) at 245 rpm for 2 h.

To make dispenser printable thermoelectric composite slurries, active particles need to be mixed in polymer binder with some solvents. Epoxy resin systems are proven polymer systems and are commonly used in commercially available electrically conductive adhesives.<sup>26</sup> We used EPON 862 diglycidyl ether of bisphenol f epoxy together with methylhexahydrophthalic anhydride MHPA (Dixie Chemicals, Inc.) hardener as the epoxy resin system. The ratio of epoxy-to-hardener was 1:0.85 based on the epoxide equivalent weight of the resin and the hydroxyl equivalent weight of the hardener. 1-cyanoethyl-2-ethyl-4-methylimidazole 2E4MZCN (Sigma-Aldrich, Inc.) was used as the catalyst. 10–20 wt % of butyl glycidyl ether Heloxy 61 (Hexion Specialty Chemicals, Inc.) was employed in the resin blend as a reactive diluent to adjust the viscosity of the slurry without compromising the desired properties.

According to the percolation theory, when the volume of conductive filler particles is above certain percolation threshold, a network of conductive filler is formed throughout the composite systems.<sup>26</sup> Empirical studies, in our case, show that active particles to epoxy volume ratio should be at least 36% to 64% in order to form the conductive path. An increase in the volume ratio of active particles beyond 40% resulted in cracking of the cured film. The epoxy resin system (active particles to epoxy volume ratio of 40% to 60%) as a polymer binder resulted in compact films with high mass loading (82%) of active particles and overall good thermoelectric properties with minimal cure shrinkage.

The slurry was mixed using a vortex mixer and an ultrasonic bath to disperse the particles. The thermoelectric inks were then printed on glass substrates to form 100–120  $\mu\text{m}$  thick films using dispenser printing, and cured at 250 or 350 °C for 12 h to form solid thick films.

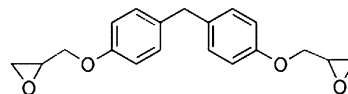


Figure 1. Bisphenol F diglycidyl ether epoxy, EPON862.

## DEVICE FABRICATION

Although TEG device geometry is highly application dependent, high-density and high-aspect-ratio arrays are frequently required for low-temperature TEG applications.<sup>9,10</sup> We use planar structure in combination with flexible substrate to achieve high packing density required to produce small size devices that can be used for low-temperature applications.<sup>24</sup> We use high-aspect-ratio device design to maintain the temperature difference across the device and to achieve reasonable power output. A flexible printed circuit board (Flex-PCB) fabricated by Rigidflex Technology Inc. was used as a substrate. The Flex-PCB consisted of nickel and gold plated copper traces on a flexible polyimide substrate. A polyimide substrate with metal electrodes was chosen due to its flexibility, electrical insulation, high temperature tolerance, and low thermal conductivity (0.12 W/m-K). Next, the MA n-type  $\text{Bi}_2\text{Te}_3$  composite inks were dispenser printed onto the substrate to form lines spanning across the top and the bottom contacts. Thick metal contacts resulted in reduced electrical contact resistance between metal contacts and printed TE elements. Printed lines on the flex PCB was cured in an argon/vacuum oven at 300 °C. 24AWG copper wires were attached to the device using conductive silver epoxy (1901-S, ESL Electroscience) to form electrical connections. A schematic of single TE elements and dispenser printed 62-element prototype consisting of elements that were 5 mm  $\times$  700  $\mu\text{m}$   $\times$  120  $\mu\text{m}$  in dimensions is shown in Figure 2.

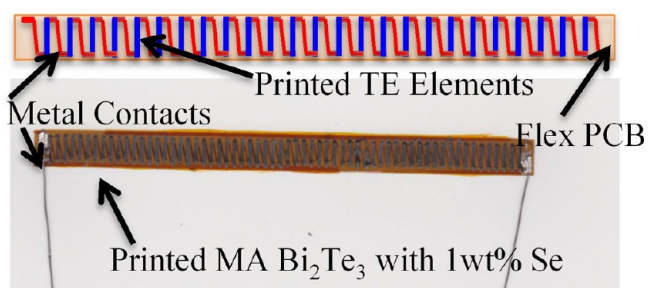
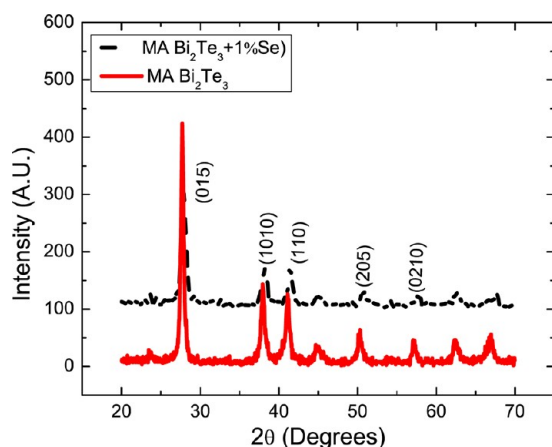


Figure 2. Schematic and image of dispenser printed 62-element MA  $\text{Bi}_2\text{Te}_3$  with 1 wt % extra Se planar thermoelectric device on a flexible substrate.

## MEASUREMENTS

X-ray powder diffraction (XRD) was performed on both MA  $\text{Bi}_2\text{Te}_3$  powder and MA  $\text{Bi}_2\text{Te}_3$  with 1 wt % Se powder. The XRD pattern is as shown in Figure 3 and can be indexed to  $\text{Bi}_2\text{Te}_3$  (JCPDF, no. 15–0863). The XRD pattern of MA  $\text{Bi}_2\text{Te}_3$  with 1 wt % Se indicates that, the majority of the  $\text{Bi}_2\text{Te}_3$  and Se reacted with each other to form  $\text{Bi}_2\text{Te}_{(3-x)}\text{Se}_x$  solid solution during mechanical alloying.<sup>27–29</sup> This is why the XRD



**Figure 3.** X-ray powder diffraction (XRD) patterns of MA  $\text{Bi}_2\text{Te}_3$  with 1 wt % extra Se thermoelectric powders.

peaks in Figure 3 shift slightly to larger angles. However, the crystal structure (rhombohedral) of  $\text{Bi}_2\text{Te}_3$  with space group (R3 m) remains unchanged; Se substitutes Te sites only.<sup>27–29</sup>

Figure 4 shows the scanning electron microscope (SEM) of  $\text{Bi}_2\text{Te}_3$  powder and average particle size is about 2  $\mu\text{m}$ .

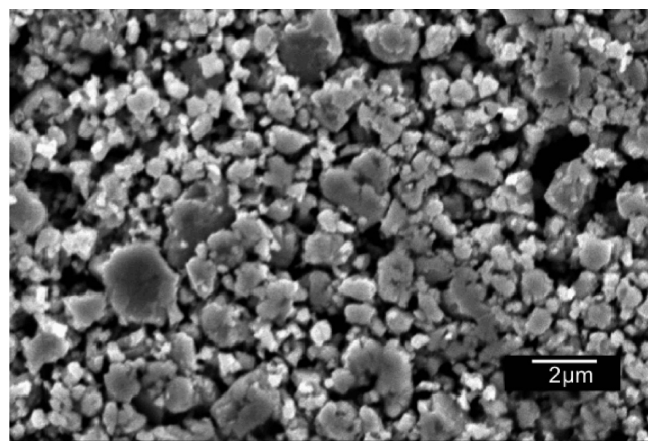


**Figure 4.** SEM micrographs of MA  $\text{Bi}_2\text{Te}_3$  confirming average particle size less than 2  $\mu\text{m}$ .

Differential Scanning Calorimeter (DSC, model 2920, TA Instruments) was used to study the melting point of MA  $\text{Bi}_2\text{Te}_3$  with 1 wt % Se sample. An endothermic reaction was observed at 425  $^{\circ}\text{C}$ , as shown in Figure 5. The DSC analysis was carried out in the air. The constant increase in the entire temperature range in Figure 5 is possibly due to oxidation of the sample.

The morphology of grains and grain boundaries of this DSC sample was analyzed using scanning electron microscope (JSM-6490 LV), as shown in Figure 6a. This SEM image suggests that MA  $\text{Bi}_2\text{Te}_3$  with 1 wt % Se melts at much lower temperature (425  $^{\circ}\text{C}$ ) than stoichiometric  $\text{Bi}_2\text{Te}_3$  (580  $^{\circ}\text{C}$ ).<sup>22</sup> However, since epoxy disintegrates at 400  $^{\circ}\text{C}$ ,<sup>19</sup> we did one more DSC of the MA  $\text{Bi}_2\text{Te}_3$  with 1 wt % Se heated till 350  $^{\circ}\text{C}$  to check possibility of grain coalescence. The SEM image of this DSC sample (heated to 350  $^{\circ}\text{C}$ ) is shown in Figure 6b confirms the grain coalescence at lower temperature. Therefore, dispenser printed composite films were cured at temperatures 250, 300, and 350  $^{\circ}\text{C}$  to verify the grain coalescence effect in epoxy polymer matrix. Figure 7 shows scanning electron microscope (SEM) images of an MA  $\text{Bi}_2\text{Te}_3$  with 1 wt % Se/epoxy

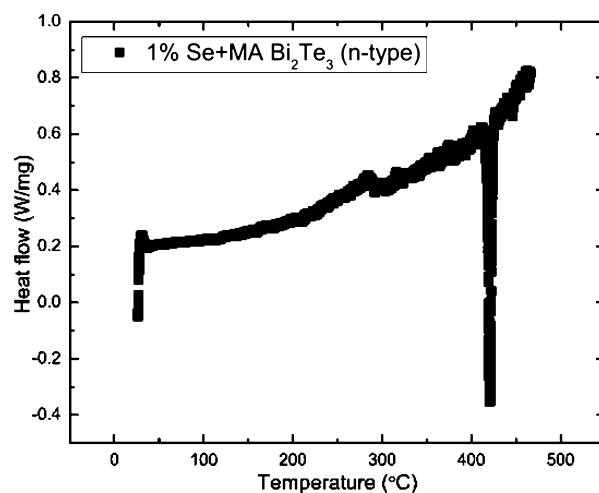


**Figure 5.** Differential scanning calorimeter (DSC) curves of MA  $\text{Bi}_2\text{Te}_3$  with 1 wt % extra Se thermoelectric powders.

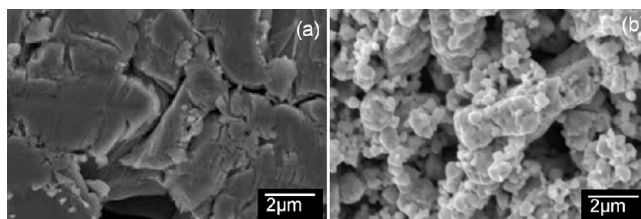


**Figure 6.** SEM micrograph of MA  $\text{Bi}_2\text{Te}_3$  with 1 wt % Se powder (DSC sample) heated to (a) 475 and (b) 350  $^{\circ}\text{C}$ .

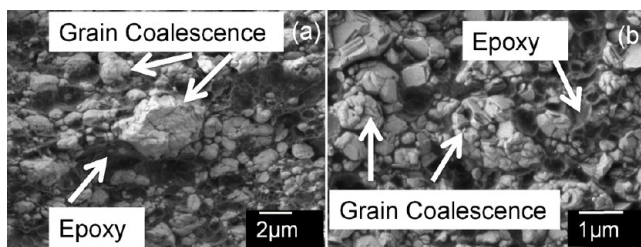


**Figure 7.** SEM micrographs of MA  $\text{Bi}_2\text{Te}_3$  with 1 wt % Se epoxy composites cured at 350  $^{\circ}\text{C}$ .

dispenser printed composite film cured at 350  $^{\circ}\text{C}$ .  $\text{Bi}_2\text{Te}_3$  grains are uniformly dispersed in the epoxy matrix. Epoxy serves to hold the  $\text{Bi}_2\text{Te}_3$  grains together in the cured film. EDS has also confirmed that amorphous areas are rich in insulating carbon confirming the presence of epoxy. Burning off the epoxy by curing the composite films at higher temperature of 400  $^{\circ}\text{C}$  (disintegration temperature of epoxy) resulted in cracking of the film. Figure 7 also suggests that even though epoxy is present in composite films but grain coalescence is still taking place.

Electrical resistivity and Seebeck measurements of the printed thermoelectric films were carried out using a custom testing device. The Hall coefficients and carrier concentration of the samples were measured at room temperature using an Ecopia HMS-3000 Hall effect measurement system; a magnetic field of 0.6 T and electrical current of 10 mA were applied. The thermal conductivity of composite samples was measured using transient plane source with a C-Therm TCi thermal conductivity analyzer. Relatively larger cylindrical-shaped



samples with 13 mm diameter were used for thermal conductivity measurements.

The printed prototype device was tested using a custom testing apparatus as shown in Figure 8 Thermoelectric heater/

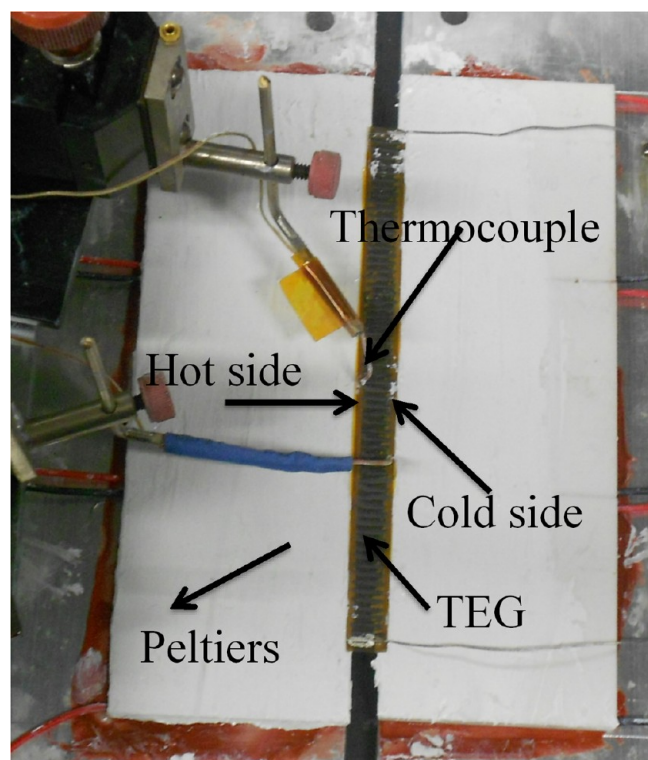


**Figure 8.** Image of thermoelectric device characterization custom-built setup.

coolers (9500/127/040 B, Ferrotech Corp.) were mounted onto two aluminum plates to provide surfaces for cooling and heating. The printed TEG was positioned between the plates and a temperature difference was applied across the device. Once the device reached steady state, the open circuit voltage of the device was measured using a digital multimeter. A variable load resistance was then connected in series with the device and voltage measurements were taken at multiple load resistances. The power was calculated based on the measured voltage and load resistance at various temperature differences.

## RESULTS AND DISCUSSION

Figure 9 shows the thermoelectric properties of MA n-type  $\text{Bi}_2\text{Te}_3$  composite films cured at 250 and 350 °C for 12 h measured at room temperature, as a function of %Se added. The curing temperatures and curing time of 12 h were chosen based on previous results for p-type  $\text{Sb}_2\text{Te}_3$ /epoxy composite films.<sup>19</sup> It is clear from Figure 9a that electrical conductivities of composite films are much lower than that of bulk  $\text{Bi}_2\text{Te}_3$ .<sup>19</sup> This decrease in the electrical conductivity can be attributed to the presence of the insulating polymer phase. Effective-medium-theory (EMT) explains the decrease in electrical conductivity due to presence of insulating polymer phase.<sup>30–32</sup> Another possible reason may be a decrease in the charge carrier mobility due to grain boundary scattering.<sup>33</sup>

As shown in Figure 9a, the addition of 1 wt % Se resulted in significant improvement in the electrical conductivity of composite films compared to without Se additive MA  $\text{Bi}_2\text{Te}_3$

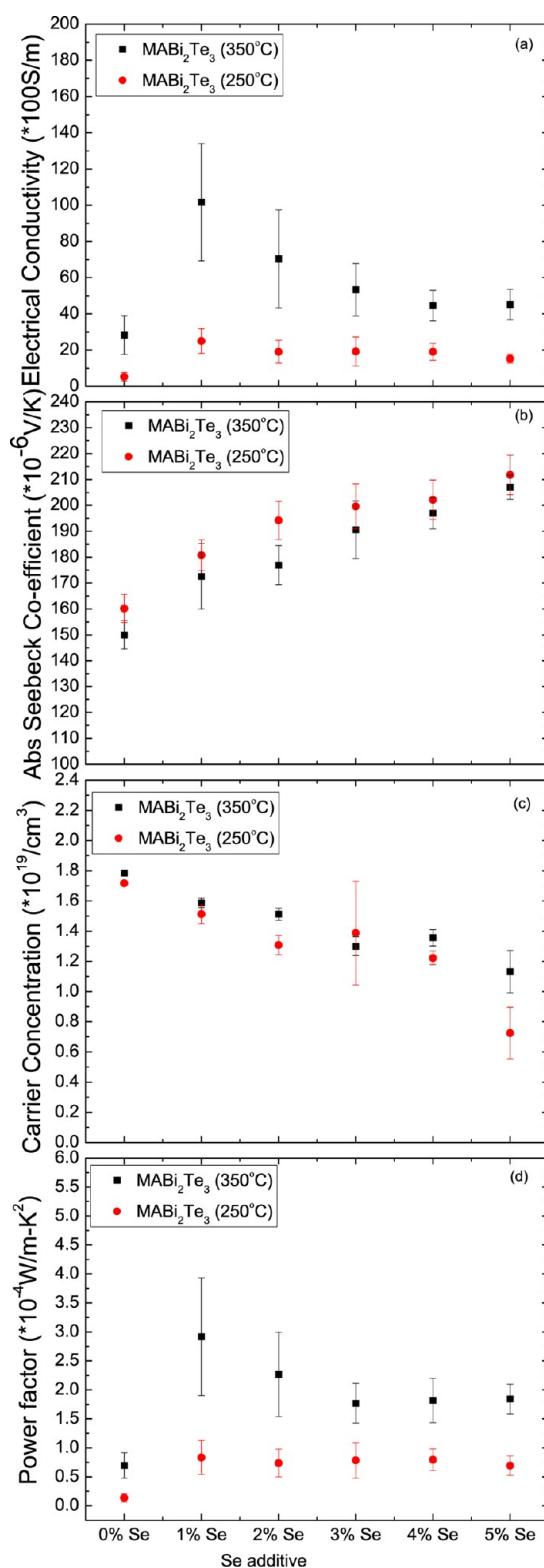


**Figure 9.** Thermoelectric properties of MA  $\text{Bi}_2\text{Te}_3$  dispenser printed composite films as a function of Se as an additive including (a) electrical conductivity, (b) Seebeck coefficient, and (c) power factor.

composite films. This improvement in the electrical conductivity is likely due to the following mechanism. Se substitutes Te sites due to weaker  $\text{Te}^{(1)}\text{—Bi—Te}^{(2)}$ —Bi—Te bonds and becomes  $\text{Te}^{(1)}\text{—Bi—Se—Bi—Te}$  or  $\text{Se—Bi—Te}^{(2)}\text{—Bi—Te}$ , leaving extra Te available to melt at lower temper-

atures.<sup>22</sup> The DSC curve of 1%Se Bi<sub>2</sub>Te<sub>3</sub> in Figure 5 shows that melting of this sample occurs at 425 °C rather than at 580 °C, the standard melting temperature of Bi<sub>2</sub>Te<sub>3</sub>. This melting is also verified by SEM micrograph of the DSC sample as shown in Figure 6a. The lower melting point helps in grain coalescence and formation of larger grains at lower sintering temperatures of 350 °C as shown in Figure 6b. This increase in grain size as a result of adding 1% Se is also observed for dispenser printed composite films as shown in Figure 7. These larger grains result in reduction in grain boundary scattering and improve mobility of carriers. The mobility of the 1%Se sample cured at 350 °C was found to be (24 cm<sup>2</sup>/(V s)), which is four times higher than (6 cm<sup>2</sup>/(V s)) mobility of undoped sample cured at 350 °C. As a result, electrical conductivity increases because of addition of 1% Se.

The electrical conductivity did not improve with increase in Se wt% beyond 1%. This is likely due to an increase in the band gap of MA Bi<sub>2</sub>Te<sub>3</sub> with increase in the amount of Se.<sup>20</sup> The melting point of Se doped Bi<sub>2</sub>Te<sub>3</sub> does not decrease with adding more Se.<sup>22</sup> Therefore, there are no further gains in mobility due to addition of Se. But, an increase in band gap lowers carrier concentration causing lower conductivity.

The electrical conductivity of samples cured at 250 °C is lower compared to samples cured at 350 °C due to curing temperatures being much smaller than melting point of the MA Bi<sub>2</sub>Te<sub>3</sub>. The highest electrical conductivity (140 S/cm) was achieved for 1 wt % Se-doped MA Bi<sub>2</sub>Te<sub>3</sub> composite films cured at 350 °C.

This electrical conductivity is still an order of magnitude lower than the bulk Bi<sub>2</sub>Te<sub>3</sub>, mainly because of leftover epoxy in the composite films cured at 350 °C. The presence of epoxy in the composite films cured at 350 °C is verified using SEM as shown in Figure 7.

Figure 9b shows variation of Seebeck coefficient with respect to Se wt%. The negative values confirm the synthesized powder as an n-type material. Seebeck coefficient decreases with increase in carrier concentration for single phase system (1). However, Seebeck coefficient of two-phase composite system, estimated by effective-medium-theory (EMT), also depend on effective electrical and thermal conductivity of composite system.<sup>31,32,34</sup>

$$\alpha = 6k \frac{\langle \alpha_j D_j \rangle}{1 - 3\langle k_j D_j \rangle} \quad (1)$$

and

$$D_j = \frac{\sigma_j}{(k_j + 2k)(\sigma_j + 2\sigma)} \quad (2)$$

where  $k$  and  $\sigma$  are effective thermal and electrical conductivities of the composite system and can be obtained by the EMT as follows

$$\left\langle \frac{\sigma_j - \sigma}{\sigma_j + 2\sigma} \right\rangle = 0 \quad (3)$$

$$\left\langle \frac{k_j - k}{k_j + 2k} \right\rangle = 0 \quad (4)$$

where the subscript  $j$  denotes the  $j$ th phase and  $\langle \rangle$  denotes volume average property parameters. Electrical conductivity of

insulating polymer epoxy is zero. Equation 1 can, therefore, be simplified as

$$\alpha = \alpha_1 \quad (5)$$

Therefore, effective Seebeck coefficient of composite system is same as single phase system (MA Bi<sub>2</sub>Te<sub>3</sub>) and related to carrier concentration.<sup>31,32,34</sup> The Seebeck coefficients of MA Bi<sub>2</sub>Te<sub>3</sub> composite films are lower (170  $\mu$ V/K) than that of Se doped MA composite printed films (200  $\mu$ V/K) cured at both 250 and 350 °C. The reason for lower Seebeck coefficients without Se is the high carrier concentration of MA Bi<sub>2</sub>Te<sub>3</sub> composite films as shown in Figure 9c. The addition of Se as a dopant reduces the carrier concentration; therefore Seebeck coefficient increases.<sup>21</sup> The absolute Seebeck coefficient for printed composite films cured at 250 °C was found to be slightly higher than that of films cured at 350 °C. However, the mechanisms involved for Seebeck coefficient improvement while curing at 250 and 350 °C are different. During the mechanical alloying process, donor-type defects are likely to be generated which provide excess n-type carriers. These defects decrease with increasing annealing time, resulting in an overall decrease in carrier concentration.<sup>35</sup> Therefore, films cured at 250 °C for 12 h have Seebeck coefficients that are similar to bulk values. However, Te is volatilized at 350 °C and bismuth oxides formed, producing antisite defects as well as Te vacancy. This increases hole carrier concentration. As a result, donor-like defect carrier concentration gets compensated by hole concentration, leading to an increase in the Seebeck coefficient.<sup>35–37</sup>

Figure 9c shows the carrier concentration measurements at 250 and 350 °C. It confirms that films cured at 350 °C have higher carrier concentration as compared to films cured at 250 °C. Also, it is clear that Se addition reduces the carrier concentration. Therefore, the Seebeck coefficient increases.

The power factor ( $\alpha^2\sigma$ ) is found to be highest for MA Bi<sub>2</sub>Te<sub>3</sub> with 1 wt % Se cured at 350 °C (4.7e-4 W/(m K<sup>2</sup>)) as shown in Figure 9d. The average thermal conductivities of MA Bi<sub>2</sub>Te<sub>3</sub> with 1 wt % Se cured at 250 and 350 °C were 0.26 W/(m K) and 0.38 W/(m K), respectively, which is almost one-third of the bulk values.<sup>19</sup> The low thermal conductivity values relative to bulk materials (typically  $\sim$ 1.2 W/(m K)) are due to the insulating nature of epoxy and fine grains of active filler particles.<sup>9</sup> A maximum ZT value of 0.31 is obtained for 1 wt % Se MA Bi<sub>2</sub>Te<sub>3</sub> dispenser printed composite films. This ZT value is higher than reported ZT of N type composite thermoelectric materials.<sup>4–8,19,25</sup>

**Table 1. Thermal Conductivity and ZT Values for Composite Thermoelectric Materials**

composite material	curing temp. (°C)	thermal conductivity (W/(m K))	ZT
MA Bi <sub>2</sub> Te <sub>3</sub> (1% Se)	250	0.26	0.15
MA Bi <sub>2</sub> Te <sub>3</sub> (1% Se)	350	0.38	0.31

To investigate the temperature dependent thermoelectric properties of composites, we measured the electrical conductivity and Seebeck coefficient of MA n-type Bi<sub>2</sub>Te<sub>3</sub> with 1 wt % Se. Figure 10 shows the thermoelectric properties of 1 wt % Se MA n-type Bi<sub>2</sub>Te<sub>3</sub> composite films cured at 250 °C, 300 and 350 °C as a function of temperature. Panels a and b in Figure 10 show that the electrical conductivity and the Seebeck coefficient do not change with the change in temperature in the

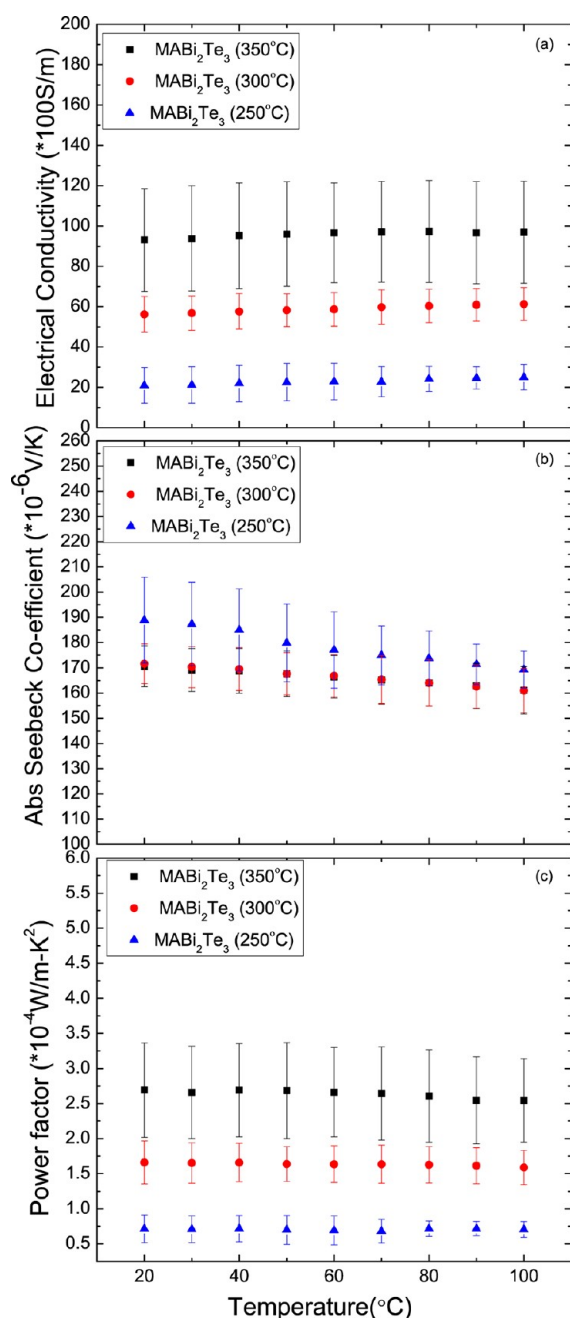


**Figure 10.** Thermoelectric properties of MA Bi<sub>2</sub>Te<sub>3</sub> with 1 wt % extra Se dispenser printed composite films as a function of temperature including the (a) electrical conductivity, (b) Seebeck coefficient, and (c) power factor.

range of 20 to 90 °C. Figure 10(c) shows that power factor ( $\alpha^2\sigma$ ) does not change with temperature in the same temperature range. Therefore, the thermoelectric properties of composite films are not adversely affected in the temperature range of 20 to 90 °C. Therefore, the TEG device made using dispenser printed composite films can be used in above-mentioned temperature range.

## ■ PROTOTYPE RESULTS AND DISCUSSION

Although highest ZT was achieved when composite films were cured at 350 °C we chose to cure the device at 300 °C. At 350 °C, cracking of films and epoxy disintegration was observed to

some extent. The device resistance of the prototype was 480  $\Omega$  when cured at 300 °C.

Figure 11 shows the device characteristic curve for the 62-element prototype device measured for  $\Delta T = 20$  K at various

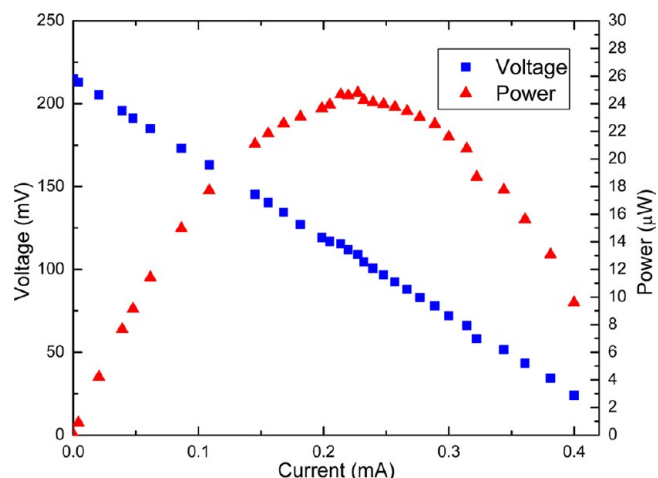


**Figure 11.** Characteristics curve of the 62 element TEG device at  $\Delta T = 20$  K.

load resistances. The optimal power output of the device occurs when the load resistance matches the device resistance.

$$P_{\max} = \frac{V_{\text{op}}^2}{4R_{\text{in}}} \quad (6)$$

Where  $V_{\text{op}}$  is the open circuit voltage and it depends on number of couples  $m$ , Seebeck coefficient  $\alpha$  and temperature difference  $\Delta T$ . The internal resistance of the device  $R_{\text{in}}$  can be estimated as

$$R_{\text{in}} = \rho \frac{L}{A} \quad (7)$$

where  $\rho$  is the electrical resistivity of the material,  $L$  (5 mm) is the element length in the direction of heat flow and  $A$  ( $700 \mu\text{m} \times 120 \mu\text{m}$ ) is the cross-sectional area of the element. The internal device resistance is very close to the expected resistance calculated from the material properties. In our previous reported papers<sup>24,25</sup> contact resistance was a big issue and caused high device resistance. However, this issue has been overcome by using the custom built flex PCB circuit with thick metal contacts. At matched load resistance, the device produces approximately 25  $\mu\text{W}$  at 0.23 mA and 109 mV closed circuit voltage.

Figure 12 shows the measured power density (power output per unit area) of the device as a function of the temperature difference. Maximum power output at matched load resistance was measured at  $\Delta T$  of 5K, 10K and 20K. The solid line in figure indicates the ideal model while the dashed line indicates the fitted model.<sup>23,38,39</sup> In the case of the fitted model,  $R_{\text{in}}$  was the measured resistance of the generator. For ideal model, power has been calculated based on intrinsic properties ( $\alpha$  and  $\sigma$ ) of dispenser printed MA Bi<sub>2</sub>Te<sub>3</sub> with 1 wt % Se films cured at 300 °C. Fitted model and actual measured power density value closely matched to ideal model at  $\Delta T$  of 5K, 10K. The modeling suggests that a device with current material properties is capable of achieving a power density of 135  $\mu\text{W}/\text{cm}^2$  given negligible contact resistance at  $\Delta T$  of 20K. However, at  $\Delta T$  of



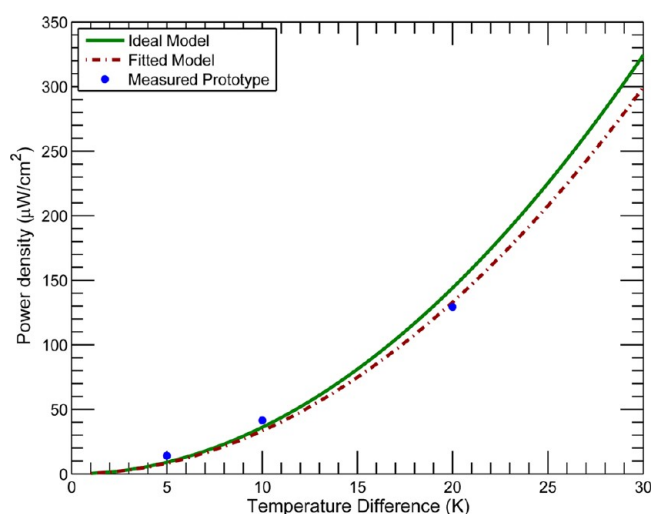


**Figure 12.** Power density at matched load resistance as a function of temperature difference across the TEG for ideal TEG model (solid line), fitted model (dotted line), measured device (diamond shape).

20K actual measured power density ( $130 \mu\text{W}/\text{cm}^2$ ) is slightly lower than ideal model ( $135 \mu\text{W}/\text{cm}^2$ ). The deviation may be due to fluctuations in temperature across the device during measurement and minor electrical contact resistance. It is worth noting that  $P_{\text{max}}$  is proportional to  $(\Delta T)^2$  because  $P_{\text{max}}$  depends on open circuit voltage as in eq 6 and open circuit voltage depends on  $(\Delta T)$ . In previous work, power output for 50-coupled device is  $10.5 \mu\text{W}$  at  $\Delta T=20\text{K}$  and power density is  $75 \mu\text{W}/\text{cm}^2$ . As a result of improving the materials properties and contact resistance, a power output of  $25 \mu\text{W}$  was achieved at  $\Delta T=20\text{K}$  and power density  $130 \mu\text{W}/\text{cm}^2$  for 62 single leg n-type device. This power density is considerably higher than  $0.27 \mu\text{W}/\text{cm}^2$  for  $\Delta T=30\text{K}$  reported in the literature using similar printing techniques.<sup>40</sup> A nonoptimized planar geometry was chosen for demonstration purposes. For specific applications, it is possible to design the TEG device to optimize the power output for various temperature differences.

This power is sufficient to power thermoelectric generator to provide adequate power for a wireless sensor/transmitter used in the health monitoring of the equipment on aircraft, aerospace, power plant, process plant industries. Higher output voltage and higher power is desired for the operation of many electronic devices. Integration with p-type element and by increasing the number of couples, higher performance of device can be easily achieved.

## CONCLUSION

In summary, enhanced thermoelectric properties have been achieved in MA n-type  $\text{Bi}_2\text{Te}_3$  with 1 wt % Se printable composite materials. Improvements in ZT were obtained by sintering effects occurring at  $350^\circ\text{C}$ , which improved the electrical conductivity. At the same time, Seebeck coefficients similar to bulk values were retained, which helps give a high overall power factor. The ZT was enhanced by the low thermal conductivity of the composite material. The ease of processing and device fabrication with printed materials provides deployment advantages over other thermoelectric materials. A 62-element planar prototype device was printed on a custom designed flexible polyimide substrate to form a TEG. The device produced  $25 \mu\text{W}$  at  $0.23 \text{ mA}$  and  $109 \text{ mV}$  for  $20 \text{ K}$  temperature difference. These results indicate an areal power

density of  $130 \mu\text{W}/\text{cm}^2$ , which is quite close to ideal power density  $135 \mu\text{W}/\text{cm}^2$ . The results shown are promising for the use of low-cost and scalable TEGs for various low-power energy harvesting applications. Further work will continue to optimize complementary p-type material to fabricate an n and p-type TEG.

## AUTHOR INFORMATION

### Corresponding Author

\*E-mail: deepam@berkeley.edu. Tel.: 510-387-5139.

### Notes

The authors declare no competing financial interest.

## ACKNOWLEDGMENTS

The authors thank the California Energy Commission for supporting this research under contract 500-01-43. We also thank Michael Nill, Jonathan Brown, Brian Mahlstedt, Kevin Huang, and Rich Winslow for their contributions.

## REFERENCES

- (1) Goldsmid, H. J.; Douglas, R. W. *Br. J. Appl. Phys.* **1954**, *5*, 386–390.
- (2) Chen, G.; Dresselhaus, M. S.; Dresselhaus, G.; Fleurial, J. P.; Calliat, T. *Int. Mater. Rev.* **2003**, *48*, 45–66.
- (3) Tritt, T. M.; Boettner, H.; Chen, L. *MRS Bull.* **2008**, *33*, 366–368.
- (4) See, K. C.; Feser, J. P.; Chen, C. E.; Majumdar, A.; Urban, J. J.; Segalman, R. A. *Nano Lett.* **2010**, *10*, 4664–4667.
- (5) Navone, C.; Soulier, M.; Plissonnier, M.; Seiler, A. L. *J. Electron. Mater.* **2009**, *39*, 1755–1759.
- (6) Xi, X.; Matijasevic, G.; Ha, L.; Baxter, D. *Mater. Res. Soc. Symp. Proc.* **1999**, 545.
- (7) Weber, J.; Potje-Kamloth, K.; Haase, F.; Detemple, P.; Volklein, F.; Doll, T. *Sens. Actuators, A* **2006**, *132*, 325–330.
- (8) Zhang, B.; Sun, J.; Katz, H.; Fang, F.; Opila, R. L. *ACS Appl. Mater. Interfaces* **2010**, *2*, 3170–3178.
- (9) Glatz, W.; Muntwyler, S.; Hierold, C. *Sens. Actuators, A* **2006**, *132*, 337–345.
- (10) Strasser, M.; Aigner, R.; Franosch, M.; Wachutka, G. *Sens. Actuators, A* **2002**, *98*, 535–542.
- (11) Bottner, H.; Nurnus, J.; Schubert, A.; Rowe, D. M. *Thermoelectrics Handbook*; Taylor and Francis: Boca Raton, FL, 2005; Chapter 46: Micro to Nano; pp 1–18.
- (12) Venkatasubramanian, R.; Colpitts, T.; Watko, E.; Lamvik, M.; El-Masry, N. *J. Cryst. Growth* **1997**, *170*, 817–821.
- (13) Noro, H.; Sato, K.; Kagechika, H. *J. Appl. Phys.* **1993**, *73*, 1252–1260.
- (14) <http://ei.haas.berkeley.edu/c2m/pdf/2011EndofYearSlides/ThermoelectricMaterial.pdf> Accessed: Nov. 2, 2012.
- (15) Ho, C. C.; Evans, J. W.; Wright, P. K. *J. Micromech. Microeng.* **2010**, *20*, 104009.
- (16) Wright, P. K.; Dornfeld, D. A.; Chen, A.; Ho, C. C.; Evans, J. W. *Trans. NAMRI/SME* **2010**, *38*, 555–561.
- (17) Wang, Z.; Chen, A.; Winslow, R.; Madan, D.; Juang, R. C.; Evans, J. W.; Wright, P. K. *J. Micromech. Microeng.* **2012**, *22*, 094001.
- (18) Koplow, M.; Chen, A.; Steingart, D.; Wright, P. K.; Evans, J. W. *Proceedings of 5th International Workshop on Wearable and Implantable BSN*; Hong Kong, June 1–3, 2008; IEEE: Piscataway, NJ, 2008.
- (19) Madan, D.; Chen, A.; Wright, P. K.; Evans, J. W. *J. Appl. Phys.* **2011**, *109*, 034904.
- (20) Miller, G. R.; Li, C. Y.; Spencer, C. W. *J. Appl. Phys.* **1962**, *34*, 1398–1400.
- (21) Hyun, D. B.; Hwang, J. S.; Ohh, T. S.; Shima, J. D.; Kolomoets, N. V. *J. Phys. Chem. Solids* **1998**, *59*, 1039–1044.
- (22) Scherrer, S.; Scherrer, H.; Rowe, D. M. *Thermoelectrics Handbook*; Taylor and Francis: Boca Raton, FL, 2005; Chapter 27: Micro to Nano, pp 1–19.



- (23) Chen, A.; Madan, D.; Koplow, M.; Wright, P. K.; Evans, J. W. *Proceedings of Power MEMS*; Washington, D.C., Dec 1–4, 2009 ; Transducers Research Foundation: San Diego, CA, 2009.
- (24) Chen, A.; Madan, D.; Wright, P. K.; Evans, J. W. *J. Micromech. Microeng.* **2011**, *21*, 104006.
- (25) Madan, D.; Chen, A.; Wright, P. K.; Evans, J. W. *J. Electron. Mater.* **2012**, *41*, 1481–1486.
- (26) Lu, D.; Tong, Q. K.; Wong, C. P. *IEEE Trans. on Electron. Packag. Manuf.* **1999**, *22*, 223–227.
- (27) Yang, J. Y.; Aizawa, T.; Yamamoto, A.; Ohta, T. *J. Alloys Compd.* **2000**, *312*, 326–330.
- (28) Yashima, I.; Watanabe, H.; Ogisu, T.; Tsukuda, R.; Sato, S. *Jpn. J. Appl. Phys.* **1998**, *37*, 2472–2473.
- (29) Du, Y.; Cai, K. F.; Li, H.; An, B. J. *J. Electron. Mater.* **2011**, *40*, 518–522.
- (30) McLachlan, D. S.; Blaszkiewicz, M.; Newnham, R. E. *J. Am. Ceram. Soc.* **1990**, *73*, 2187–2203.
- (31) Nan, C. W. *Prog. Mater. Sci.* **1993**, *37*, 1–116.
- (32) Webman, I.; Jortner, J. *Phys. Rev. B* **1977**, *16*, 2564–2959.
- (33) Das, R. N.; Papathomas, K. I.; Lauffer, J. M.; Egitto, F. D. *Proceedings of the 57th Electronic Components and Technology Conference*; IEEE: Piscataway, NJ, 2007; pp 74–81.
- (34) Zhao, L. D.; Zhang, B. P.; Liu, W. S.; Zhang, H. L.; Li, J. F. *J. Alloys Compd.* **2009**, *467*, 91–97.
- (35) Zhao, L. D.; Zhang, B. P.; Li, J. F.; Zhou, M.; Liu, W. S. *Phys. B* **2007**, *400*, 11–15.
- (36) Stary, Z.; Hora, J. k.; Stordeur, M.; Stolzer, M. *J. Phys. Chem. Solids* **1988**, *49*, 29–34.
- (37) Miller, G. R.; Li, C. Y. *J. Phys. Chem. Solids* **1965**, *26*, 173–177.
- (38) Strasser, M.; Aigner, R.; Lauterbach, C.; Sturm, T. F.; Franosch, M.; Wachutka, G. *Sens. Actuators, A* **2004**, *114*, 362–370.
- (39) Glatz, W.; Schwyter, E.; Durrer, L.; Hierold, C. *J. Micromech. Syst.* **2009**, *18*, 763–772.
- (40) Bubnova, O.; Khan, Z. U.; Malti, A.; Braun, S.; Fahlman, M.; Berggren, M.; Crispin, X. *Nat. Mater.* **2011**, *10*, 429–433.